Journal of Sound and Vibration (2002) **252**(1), 115–139
doi:10.1006/jsvi.2001.4029, available online at http://www.idealibrary.com on IDEAL®

A WAVENUMBER APPROACH TO MODELLING THE RESPONSE OF A RANDOMLY EXCITED PANEL, PART II: APPLICATION TO AIRCRAFT PANELS EXCITED BY A TURBULENT BOUNDARY LAYER

C. Maury, P. Gardonio and S. J. Elliott

Institute of Sound and Vibration Research, University of Southampton, Southampton SO17 1BJ, England. E-mail: cm@isvr.soton.ac.uk

(*Received* 15 *December* 2000, *and in final form* 30 *August* 2001)

Part I of this paper has shown the suitability of wavenumber–frequency approach in the calculation of the vibro-acoustic response of a thin baffled plate to a large class of random excitations. Part II describes the application of this formulation to the prediction of the vibration and the acoustic radiation of an aircraft fuselage panel exposed to boundary layer turbulence.

The first section briefly describes the modelling of the wall-pressure fluctuations and justifies as to why a Corcos-like model for the wall-pressure field is suitable for high subsonic flow applications. In the next sections, several parametric studies are presented. These are first used to verify the validity of the hypothesis underlying our simplified model. Then we examine the influence of the main physical parameters on the vibro-acoustic response of the system. Finally, the predictions of our model are compared with some previously reported experimental measurements taken on a panel excited by a turbulent boundary layer.

1. INTRODUCTION

The continual development of jet-powered, well-streamlined aircraft has driven an increasing number of studies concerning the sound and the vibration generated in the cabin by the airflow developed over the fuselage under cruise conditions [1]. More recently, the boundary layer noise induced in aircraft has received increasing attention since the contribution of other noise sources, such as the engine exhaust noise, has now been significantly reduced while maintaining optimal performance and fuel efficiency [2]. Moreover, flow-induced noise increases more rapidly with respect to the stream velocity than other noise sources and so, appears to be a particularly critical problem in transonic aircraft. Other airframe noise sources are also generated by wake vorticity beyond the fuselage or wings trailing edge, by inflow turbulence developed on aerodynamic surfaces such as flaps, inline wheels or horizontal tails located in the wake of the other aircraft portions, and by wheel cavities [3]. However, airframe noise occurs predominantly during the takeoff and the landing configurations and, because of their short duration, the subsequent discomfort is generally acceptable to the passengers.

On the other hand, because the noise generated by turbulent airflow over the surfaces of high-speed aircraft is a major source of annoyance during the long cruise portions of a flight, there is an important economic interest in reducing the transmission of boundary layer noise within the cabin. This problem has to be addressed at the design stage and

0022-460X/02/$35.00

requires a simple model, as analytic as possible, in order to save the most computational effort and provide the best physical insight.

Many studies have already been devoted to the prediction of fuselage vibration and aircraft interior noise due to the turbulent boundary layer (TBL) pressure fields. Most of the physical models [4–6] have considered a fuselage skin divided into an array of panels whose vibration is uncorrelated. The vertical and horizontal dimensions of these panels correspond to the distance between two adjacent frames and two adjacent stringers respectively. The validity of this model has been confirmed as representative by extensive flight test measurements conducted by Boeing and carried out on the forward and rear part of an airplane fuselage under cruise conditions [7, 8]. These data have shown that, from 500 Hz to 1·5 kHz, the boundary layer noise is preponderant and excites the forward part of the fuselage in such a way that the flow-induced vibrations are only correlated over a single fuselage bay in the streamwise direction. This is not the case for the rear portion where jet noise then produces highly correlated vibrations across several bays in the streamwise and in the spanwise direction at frequencies below about 800 Hz.

A second point concerning the geometry of the modelled subsystem is that the adjacent bays are set in a cylindrical fuselage and the effects of curvature have to be considered *a priori*. However, recent analytical work [9] has shown that, for subsonic applications, the influence of the panel curvature on the interior sound field can be neglected if the surrounding inner surface is sufficiently hard to appear as a baffle, but, at the same time, sufficiently absorbing to neglect the diffracted sound waves due to the curvature. These competing effects seem, *a priori*, difficult to achieve in aeronautical applications but the influence of curvature still appears to be negligible when compared with the influence of in-plane stresses acting on the boundaries of the panel [6]. These membrane tensions are due to the cabin pressurization and lead to an increase of the typical fundamental resonance frequency of each bay by a factor of about 3. Hence, the main physical characteristics of the problem are retained by considering the simplified, but relevant model of a simply supported flat plate stressed by tension forces.

The third point is related to the modelling of the structural damping effects. We will introduce an equivalent damping ratio ζ which accounts for several effects [10]: the internal material damping, usually modelled through a *hysteresis* loss factor η, and the boundary damping due to the friction in the joint edges or due to the energy lost by the panel through its elastic boundaries. We will consider in our simulations two characteristic cases: an aluminium panel which accounts both for the hysteretic damping and the energy losses through its boundaries ($\zeta = 0{\cdot}01$) and a panel which accounts for the damping effect of a "trimmed" panel [11, 12], i.e., the dissipation due to the insulating material placed between the interior trim panel and the outer fuselage skin ($\zeta = 0{\cdot}05$). However, we should keep in mind that a more rigorous modelling of the trimmed panel should address the problem of two flexible panels enclosing a cavity filled with blankets of insulating materials. Results concerning the alteration of the characteristics of turbulent boundary layer noise transmission through double panels will be presented in a forthcoming paper.

Finally, measurements performed at high Mach numbers have shown that the damping in the structural acoustic response of TBL-excited panels may vary significantly as a function of the mean-flow speed. Thus, recent investigations [13–15] have accounted for aeroelastic coupling, i.e., the influence of the mean flow on both the acoustic propagation and the fluid–structure interaction at subsonic and supersonic Mach numbers. These studies have pointed out a beneficial aerodynamic damping effect, leading to a decrease in the flow-induced noise transmitted by the fuselage mainly for increasing supersonic Mach numbers. However, this effect is overwhelmed, in practice, by an increase in the levels of the

TBL noise source, which scale on the mean-flow velocity, and also by increased transmission efficiency due to surface effects on the boundary layer pressure distribution generated over the fuselage skin, such as structural inhomogeneities and ring stiffeners [16], the wall roughness [17] and step-like discontinuities [18]. An important point is to know the parameter range over which the influence of aeroelastic coupling can be neglected. This point is addressed in reference [15]. It is shown that, for a typical aircraft panel, up to Mach number of 0·7, the aerodynamic damping effect can still be neglected without significantly affecting the dynamics of the system.

The model described above has allowed extensive analysis to be performed either to predict or to control flow-induced structural vibration and sound radiation inside aircraft cabins. In order to understand the airborne noise transmitted through the fuselage bays due to turbulent wall-pressure fluctuations, structural modal analysis forms the background of many investigations in the low-frequency domain and/or for simple elements, whereas statistical methods like power flow energy analysis are more suitable when considering systems which exhibit high modal densities [19]. To our knowledge, the first attempt to derive a statistical estimate of the sound power radiated by airflow-excited panels starting from a modal analysis was made by Davies [5]; the usual simplifications, such as neglecting the acoustic and the excitation coupling between the structural modes, have been required for predicting trends. Several investigations of the modal approach have been proposed by the use of space–frequency or a space–time formulation for the turbulent excitation [20–22]. Other authors have also shown the suitability of a wavenumber–frequency approach either to obtain reduced algebraic forms leading to asymptotics and analytical approximations [23–25] or to gain further insight into the coupling between a structural mode and the turbulent flow or the acoustic field [26–29]. It is also important to know the required precision for the modelling of the excitation field in order to describe the vibro-acoustic response of the structure with sufficient accuracy. A large number of publications [28–32] have been focussed on the choice of the modelling of the wall-pressure fluctuations with respect to the frequency range or the Mach number of interest.

In this paper, these excitation models will be briefly reviewed before an efficient method of modelling the response of a turbulent boundary layer-excited panel is presented, based on the wavenumber approach described in Part I of this paper. This model is then used to calculate the response for a particular and representative example of a panel for different conditions and different TBL models. The influence of these models is discussed for high subsonic Mach number applications in section 2 of the paper. Section 3 contains the results of various parametric studies. The aim is to confirm the main hypotheses of the model and to provide a better understanding of the coupling between the dynamic behaviour of the structure and flow turbulence. Finally, comparisons between our predictions and previous measurements are discussed in section 4.

2. MODEL FOR TURBULENT WALL-PRESSURE FLUCTUATIONS

Numerical predictions of TBL pressure fluctuations are limited to low Reynolds number simple flows and, in any other case one has to rely on semi-empirical models fitted to experimental data. A large number of these models have been developed to described the wall-pressure fluctuations on a rigid plane wall due to a turbulent boundary layer. A comprehensive review of the most classical models can be found in reference [31].

One of the first models was introduced by Corcos [33] to discuss problems of spatial resolution for pressure transducers at high frequency. Corcos assumed that the spectrum of the wall-pressure fluctuations can be expressed in a separable form along the spanwise and

the streamwise directions, so that, in the wavenumber–frequency domain:

$$S_{p_b p_b}(\mathbf{k};\omega) = \mathbf{\Phi}_0(\omega)\frac{L_x}{[k_x^2 L_x^2 + 1]}\frac{L_y}{[(k_y - \omega/U_c)^2 L_y^2 + 1]}, \tag{1}$$

where $U_c \approx 0{\cdot}7U_\infty$ is the eddy convection velocity and U_∞ the free-stream velocity. Measurements [34] have shown that the value of the ratio U_c/U_∞ is relatively constant with respect to frequency and to the streamwise separation variable.

In equation (1), $\mathbf{\Phi}_0(\omega)$ is the point-power spectrum defined by

$$\mathbf{\Phi}_0(\omega) = \iint_\infty S_{p_b p_b}(\mathbf{k};\omega)\,\mathrm{d}^2\mathbf{k}. \tag{2}$$

Because we are concerned with high subsonic flow applications, we have chosen the model proposed by Efimtsov [30] for the point-power spectrum since it has been determined from experimental data obtained up to high Mach numbers ($M_c \leqslant 0{\cdot}9$). It is given as a function of the Strouhal number $\mathrm{Sh} = \omega\delta/U_\mathrm{r}$ by

$$\mathbf{\Phi}_0(\omega) = \frac{\tau_\mathrm{w}^2\delta}{U_\tau}\frac{0{\cdot}01\pi}{(1 + 0{\cdot}02\mathrm{Sh}^{2/3})}, \quad U_\tau = \sqrt{\frac{\tau_w}{\rho}} \approx 0{\cdot}03\,U_\infty, \tag{3}$$

where δ is the boundary layer thickness, τ_w is the mean wall shear stress and U_τ is the friction velocity. The Strouhal number is the non-dimensioned variable associated to the boundary layer thickness.

Equation (1) for the excitation spectrum also contains the spanwise and streamwise correlation lengths, namely L_x and L_y. The following empirical expressions have been proposed by Efimtsov [30] for Mach numbers lower than 0·75:

$$L_x = \delta\left\{\left[\frac{0{\cdot}77\mathrm{Sh}}{U_c/U_\tau}\right]^2 + \frac{300^2}{\mathrm{Sh}^2 + 1648}\right\}^{-1/2}, \tag{4}$$

$$L_y = \delta\left\{\left[\frac{0{\cdot}1\mathrm{Sh}}{U_c/U_\tau}\right]^2 + \frac{5300}{\mathrm{Sh}^2 + 2235}\right\}^{-1/2}, \tag{5}$$

Unlike those used in the original Corcos model [33], they depend on the boundary layer thickness. At high Mach numbers (or low frequencies), when the wall-pressure fluctuations are correlated over large distances, the influence of the boundary layer thickness cannot be neglected whereas, at low Mach numbers (or high frequencies), expressions (4, 5) coincide with the correlation lengths proposed by Corcos.

The dimensionless wavenumber–frequency power spectrum given by references (1–5) has been plotted at 200 Hz for two Mach numbers in Figure 1. The maximum corresponds to the convective ridge. It occurs for streamwise wavenumbers $k_y \approx \omega/U_c$, and for spanwise wavenumbers $k_x \approx 0$. It separates the low-wavenumber region ($k_y U_c/\omega < 1$) from the high-wavenumber region ($k_y U_c/\omega > 1$). At high Mach number, the correlation lengths (4, 5) are much smaller than those originally proposed by Corcos and so, the convective peak is broadened (see Figure 1, thin and bold curves). The same phenomenon occurs with the Chase model described below, but to a lesser extent (Figure 1, dashed and dash-dotted curves).

By comparisons with measurements, Blake [35] has shown that the Corcos model provides a good estimate of the power spectrum of flow-noise near the convective ridge.

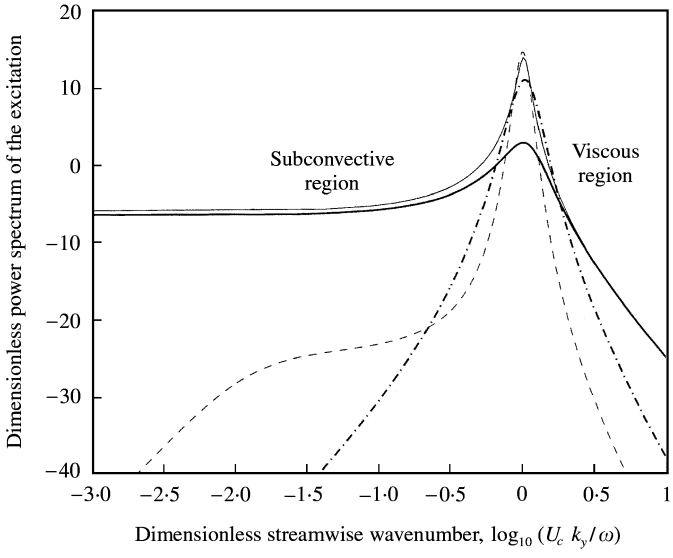

Figure 1. The dimensionless wavenumber–frequency spectrum of the excitation $\omega^2 S_{p_b p_b}(0, k_y; \omega)/U_c^2 \mathbf{\Phi}_0(\omega)$ as a function of the logarithm of the dimensionless streamwise wavenumber $k_y U_c/\omega$ at a fixed frequency, $f = 200$ Hz, and for different Mach numbers; ——, Corcos model, $M_c = 0{\cdot}7$; ——, Corcos model, $M_c = 0{\cdot}09$ -·-·-, Chase model (incompressible), $M_c = 0{\cdot}7$; - - - -, Chase model (incompressible), $M_c = 0{\cdot}09$.

This model is particularly useful for high flow speed applications like aircraft boundary layers since, in this case, the convective wavenumber ω/U_c nearly coincides with the first modal wavenumbers of the plate. This hydrodynamic coincidence phenomenon shows that an accurate modelling of the convective domain will be required for vibroacoustic predictions in this aeronautical application.

Another advantage of a Corcos-like model is that it is simple enough to provide closed-form analytical expressions for the modal excitation term, $\mathbf{\Psi}_{mn}^{pq}(\omega)$ from equation (65) in Part I, either in the space–frequency domain [20] or in the wavenumber–frequency domain [6]. Thus, extensive parametric studies can easily be handled over a wide frequency range without a lot of computational effort.

However, the Corcos model overestimates dramatically the low-wavenumber levels for the power spectrum which, then, exhibits a white wavenumber spectrum from 20 to 40 dB above the measured spectrum in the subconvective region down to the compressible (or acoustic) domain ($|\mathbf{k}| \approx \omega/c$). Specifically, in most low Mach number applications, such as underwater acoustics, for which the structural wavenumbers are usually much lower than the convective wavenumber, large eddy scales of turbulence contribute as a major part to the vibro-acoustic response of the structure and, hence, one needs a more rigorous model than the Corcos description for the low-wavenumber region. For this purpose, in 1980, Chase formulated a model [36] to describe spectral elements of the flow noise down to and near the acoustic wavenumber (Figure 1, dashed and dash-dotted curves). Blake [35] has shown that this semi-theoretical formulation agreed reasonably well with measured data within a wide range of subconvective wavenumbers down to $k_y \approx 0{\cdot}4/\delta^*$, where δ^* is the boundary layer displacement thickness.

In summary, the Chase and Corcos-like modes are complementary. The Corcos power spectrum of the excitation provides a good estimation for the levels of the wall-pressure fluctuations near and at the convective peak which is of fundamental importance for aircraft boundary layers. On the other hand, the Chase power spectrum is more suitable for

TABLE 1

Physical parameters for the aircraft panel used in the simulations

Parameters	Value
Free-stream velocity	$U_\infty = 225\ m/s$
Boundary layer thickness	$\delta = 0{\cdot}1$ m
Panel thickness	$h = 0{\cdot}0015$ m
Panel Young's modulus	$E = 7{\cdot}24 \times 10^{10}$ Pa
Panel longitudinal tension	$N_y = 29\,300$ N/m
Panel lateral tension	$N_x = 62\,100$ N/m
The panel Poisson's ratio	$\nu = 0{\cdot}33$
Panel mass density	$\rho = 2800$ kg/m^3
Panel damping ratio	$\zeta = 0{\cdot}01$ or $\zeta = 0{\cdot}05$
Panel dimensions	$a = 0{\cdot}414$ m, $b = 0{\cdot}314$ m
Sound speed in fluid	External fluid: $c_+ = 300$ m/s Internal fluid: $c_- = 340$ m/s
Fluid density	External: $\rho_+ = 0{\cdot}44$ kg/m^3 Internal: $\rho_- = 1{\cdot}2$ kg/m^3

low-speed flow applications where the strongest flow–structure interaction occurs in the low-wavenumber region. For our case of interest, with a Mach number of 0·7, a Corcos-like model of the excitation seems well suited. However, in paragraph 3.3, the influence of both the Chase and Corcos models on the sound power radiated by an aircraft panel will be presented.

3. NUMERICAL RESULTS

In this section, numerical results are presented for the response of an aircraft panel excited by a turbulent boundary layer. We have considered a tensioned aluminum panel with a thickness of 0·0015 m, which is characteristic of an aircraft with a radius of about 2 m. The aircraft is assumed to be flying at Mach 0·75, at an altitude of about 30 000 ft, which results in a differential static pressure load of 7000 N/m^2 on the fuselage panel. According to the model used by Koval [37], these values lead to initial in-plane tensions of 29 300 N/m in the axial direction and 62 100 N/m in the spanwise direction. The geometrical and mechanical parameters of the panel used in this study are summarized in Table 1.

3.1. CONVERGENCE OF THE MODAL REPRESENTATION

As outlined in the Appendix A of Part I, the bandwidth of the excitation field determines the number of modes required for the modal representation of the solution. In practice, given an upper frequency f, we can deduce the number of modes (M_{max}, N_{max}) that will contribute significantly in the modal expansion of the solution from a criteria similar to equation (A3) (Appendix A of Part I), but derived for a tensioned panel:

$$\left\{\left[\left(\frac{M_{max}}{b}\right)^2 + \left(\frac{N_{max}}{a}\right)^2\right]^2 + \frac{N_x}{D}\left(\frac{M_{max}}{b\pi}\right)^2 + \frac{N_y}{D}\left(\frac{N_{max}}{a\pi}\right)^2\right\}^{1/4} \geqslant \left(\frac{m}{D}\right)^{1/4}\sqrt{\frac{2f}{\pi}}. \quad (6)$$

Expression (6) is not easily tractable and we will prefer to determine the required number of non-resonant highly excited modes from the form of the modal excitation terms.

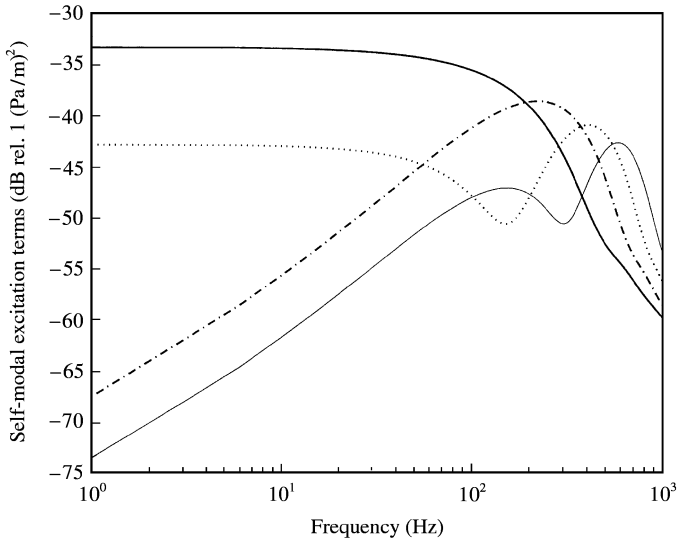

Figure 2. The self-modal excitation terms $\Psi^0_m(\omega)$ as a function of the frequency for increasing streamwise mode numbers: ———, (1, 1); - · - · -, (1, 2); · · · ·, (1, 3); ——, (1, 4).

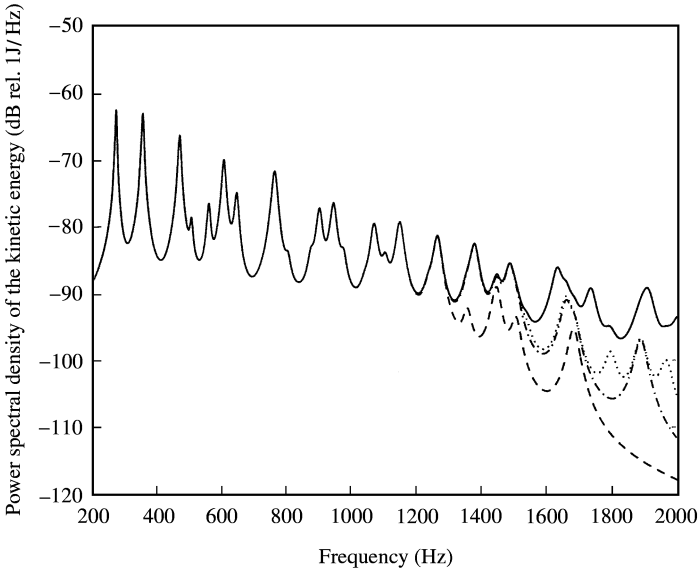

Figure 3. The power spectral density of the kinetic energy as a function of the frequency when an increasing number of structural modes is accounted for: – – – –, (3, 6), - · - · -, (3, 7); · · · ·, (4, 7); ——, (6, 10); ———, (8, 12).

Figure 2 shows the first coefficients of the self-modal excitation terms Ψ^0_{mn} of series (80) (Part I) as a function of frequency. They correspond to the projection of the excitation field on the set of eigenmodes. Using a Corcos-like model for the excitation, their analytical expression is readily obtained in the space–frequency domain [20] or in the wavenumber–frequency domain [6]. At a given frequency, the contribution of a non-resonant mode to the panel response is more important when the modal excitation term is high. This maximum value of $\Psi^0_{mn}(\omega)$ (see Figure 2) occurs, in the wavenumber

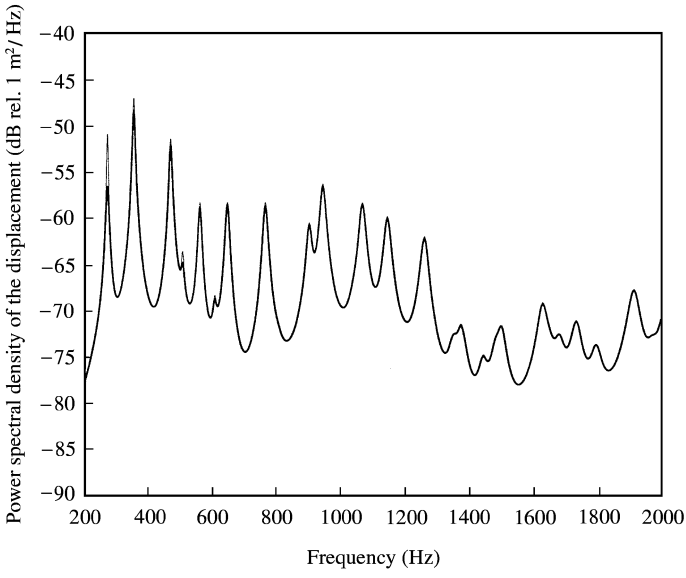

Figure 4. Fluid-loading effect on the vibrating response of an aircraft panel: ———, with fluid-loading; ——, without fluid-loading.

domain, for frequencies for which the convection peak of the turbulent pressure field nearly coincides with the maximum peak of the modal shape function at the hydrodynamic coincidence (see Figure 3 and 4 in Part I).

For the aircraft panel considered here, all the modes up to order 6 and 10, respectively, in the spanwise and streamwise directions were required to accurately describe the power spectral density of the panel response up to 2 kHz. This is illustrated in Figure 3 where the power spectral density of the panel kinetic energy has been plotted with an increasing number of structural modes accounted for. Below the convergence limit, increasing the number of streamwise modes has a significant effect on the spectrum levels over a wide frequency range while increasing the number of spanwise modes has a smaller effect.

3.2. VERIFICATION OF THE SIMPLIFYING ASSUMPTIONS

3.2.1. *The fluid-loading effect*

Figure 4 shows the spectral density of the panel displacement ($\varsigma = 0{\cdot}01$) excited by a turbulent boundary layer and calculated at the point $(x_0, y_0) = (0{\cdot}3b, 0{\cdot}2a)$ when using two different expressions. All the structural modes up to 2 kHz contribute to the response at this position. The bold curve has been plotted using the first order approximation of the panel structural response in the light fluid-loading case (see equation (63), Part I). We note that, for a typical aircraft panel described by the physical parameters given in Table 1, our frequency range of interest (up to 2 kHz) is well below the coincidence frequency (8 kHz) and the first order approximation (63) of the modal series can be applied. It is compared to the thin curve corresponding to the zero-order approximation of the panel response; in this case, equation (63) is modified according to approximations (73, 74).

Only the magnitude of the first resonance is significantly reduced because of the radiation damping effect. Also, one can see that the added mass effect, that shifts down the resonances,

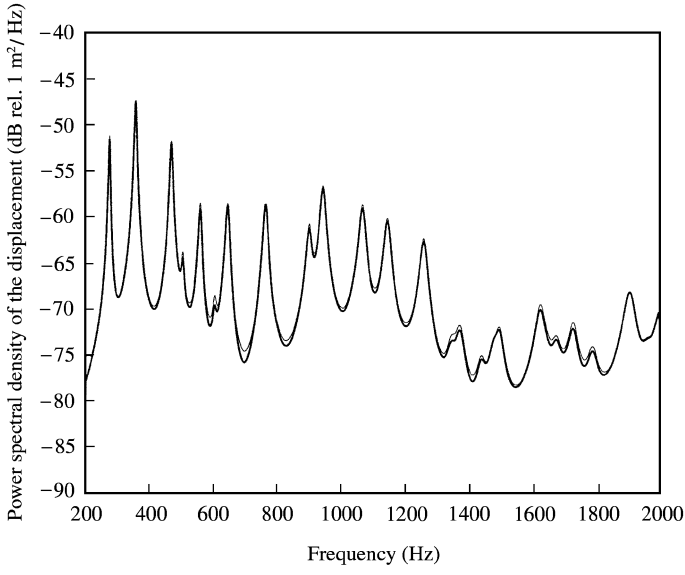

Figure 5. Comparison between the vibrating response for the full solution (———) and the diagonal solution (——).

can be clearly neglected. The same simulations have been carried out for a structural damping ratio $\zeta = 0{\cdot}05$ [38]. The same phenomena are observed, but the reduction is less pronounced at the first resonance. This is due to the fact that, in this case, the radiation damping effect becomes relatively less important with respect to the structural damping effect. In view of these initial simulations, we will neglect the radiation damping effect in the following analysis since it will not affect the main physical trends that we are going to investigate.

3.2.2. *The cross-modal excitation terms*

Figure 5 shows a comparison for the prediction of the spectral density of the panel displacement ($\zeta = 0{\cdot}01$) evaluated at the point (x_0, y_0) either from the full expansion (63) in Part I (bold curve), or from the approximate expansion deduced from equation (63) by neglecting the cross-modal excitation terms with respect to the diagonal terms (thin curve).

This example clearly shows that the cross-modal excitation terms can be neglected in the prediction of the vibrating response of this flow-excited plate over the frequency range of interest here. This could have been expected simply by looking, in Part I, at condition (79) which defines a transition frequency ($\omega_T = U_c/a\alpha_y$) above which the approximation is valid, i.e., 519 Hz in our case. One can see that the cross-terms are still negligible below ω_T because there is not a great modal overlap in this frequency range. The diagonal solution will thus be used for the simulations carried out in the rest of this section at high-speed subsonic flow.

3.3. INFLUENCE OF THE EXCITATION MODEL

In section 2, we have shown that for high subsonic flow applications a Corcos model of the TBL excitation, accounting for the dependence of the correlation lengths on the

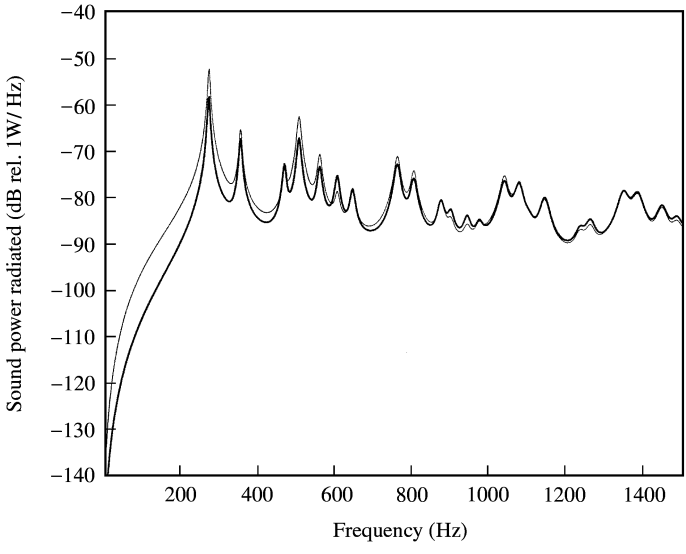

Figure 6. The sound power inwardly radiated by an aircraft panel ($\zeta = 0{\cdot}01$) when a Corcos model (———) and a Chase model (——), both at $M_c = 0{\cdot}7$, are used to describe the turbulent pressure field.

boundary layer thickness given by equations (4, 5), is more suitable than the Chase model to describe the levels of the turbulent pressure fluctuations in the neighbourhood of the convective peak. In order to verify this result, we have plotted in Figure 6 the sound power inwardly radiated by the aircraft panel when this Corcos model (bold curve) and the Chase model (thin curve) are used to represent the wall-pressure field. Up to 600 Hz, the levels predicted when using a Corcos model are lower than those obtained with the Chase model (max. 5 dB on the peaks levels). Above this frequency, the levels are quite similar. Similar results have been obtained in the case of the untensioned panel, but, in this case, the maximum difference reaches up to 10 dB at the first resonant peak.

The trends shown in Figure 6 can be explained by using the dimensionless excitation spectra in Figure 1. For a fixed high subsonic flow velocity ($U_\infty = 225$ m/s), the difference in levels at the convective peak observed between the Corcos and the Chase model in Figure 1 are responsible for the difference in levels of the sound power radiated by the panel in the low-frequency domain. The low-frequency domain is defined by the Strouhal number in section 2 being less than about 70, i.e., below about 800 Hz for $M_c = 0{\cdot}7$.

Note that the levels observed at the convective peak in Figure 1 for both the Corcos and the Chase model are quite similar for $M_c = 0{\cdot}09$ and at $f = 200$ Hz. They correspond to a Strouhal number of about 150. By using a similarity argument, the same Strouhal number is also obtained for $M_c = 0{\cdot}7$ and for $f \approx 1{\cdot}4$ kHz. Thus, under these conditions, there is also very little difference between the peak levels of the Chase and Corcos models, as observed in Figure 6.

In summary, this comparison shows that, for the aircraft panel of interest, the dependence of the correlation lengths on the boundary layer thickness cannot be neglected when describing the sound power inwardly radiated below 600 Hz. Above this frequency, neglecting this dependence leads to only small errors on the levels predicted. Although the Corcos model overpredicts the low-wavenumber levels for a TBL excitation, we note that, for a Mach number of 0·7, the choice of the Corcos model does not significantly modify the vibro-acoustic response of the panel with respect to the Chase model.

TABLE 2

Eigenfrequencies and critical frequencies of the panel (Hz)

m	*n*	Flat panel	In-plane tension	Curved, tensioned	Critical frequency
1	1	58	225·9	269·1	679·5
1	2	121·5	304·9	413·5	983·6
2	1	168·4	434·2	437·1	1158·0
1	3	227·3	425·1	548·1	1345·6
2	2	231·9	494·4	515·6	1359·0
2	3	337·7	596·3	637·7	1640·1
3	1	352·4	686·8	687·3	1675·3
1	4	375·5	584·2	687	1729·4
3	2	415·9	742·3	746·8	1820·0
2	4	485·9	740·9	791·8	1967·3
3	3	521·7	837·4	850·1	2038·5
1	5	566	782·5	867·6	2123·3
4	1	610	991	991·1	2204·2
3	4	669·9	974·2	995	2309·9
4	2	673·5	1046	1047·2	2316·1
2	5	676·4	928·4	979·9	2491·4

3.4. PARAMETRIC ANALYSES

Table 2 summarizes the values of the first eigenfrequencies of an aircraft panel considered either as a flat untensioned panel (column 3), as a flat tensioned panel (column 4) or as a curved tensioned panel (column 5). The fifth column represents the set of frequencies for which the acoustic wavelength coincides with each modal wavelength and also named the *critical frequency* of each mode.

3.4.1. *Effect of membrane stresses*

As shown in Table 2, the in-plane tensions lead to an increase of the fundamental eigenfrequency of the panel by a factor of about 3. The order of the corresponding eigenfrequencies for the individual modal values (m, n) associated with each structural mode are also modified. The corresponding mode shapes are, however, still the same as those for the untensioned panel.

Figure 7 presents a comparison of the sound power inwardly radiated by the untensioned panel (thin curve) and by the tensioned panel (bold curve) when excited by the TBL. This figure clearly confirms that we cannot neglect the influence if the in-plane tension even in a simplified model.

3.4.2. *Effect of circumferential curvature*

Table 2 (column 5) also presents the first eigenfrequencies of a curved aircraft panel which are obtained from the analytical approximations given by Blevins [39]. We have used a typical circumferential radius of 2 m [8]. One can see that the curvature raises the natural frequencies of a curved panel above that of an analogous flat plate by a factor of up to about 1·3, but in a non-uniform way. Indeed, it can be noticed, as expected, that the eigenfrequencies that are only slightly raised (less than 1%) are those associated with the very first modal order in the direction along the axis of the aircraft.

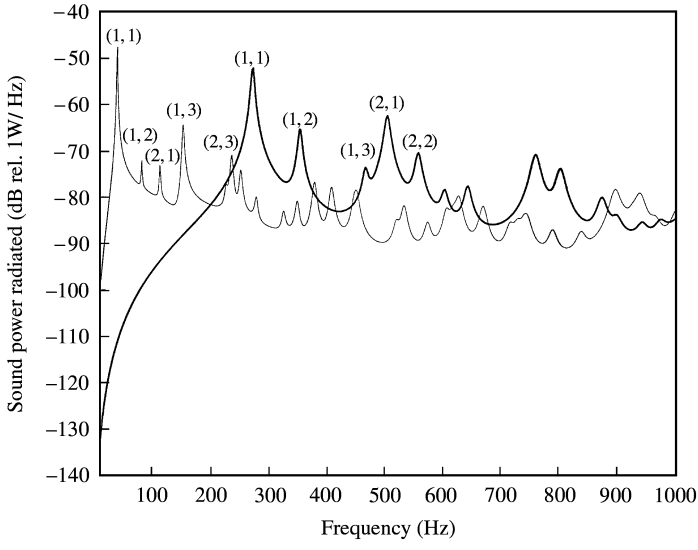

Figure 7. The sound power inwardly radiated by an aircraft panel (———) and an untensioned panel (——) when both are excited by a turbulent pressure field ($\zeta = 0{\cdot}01$).

Although the influence of curvature on the structural properties of an aircraft panel are not negligible, they are still less important than the influence of the cabin pressurization. Through investigations have been carried out to determine the effects of panel curvature on the sound field inwardly radiated [9] as well as on the wall-pressure fluctuations [40]. The effect of curvature on the acoustic radiation has already been discussed in the introduction. The effect of surface curvature on the wall-pressure fluctuations cannot be neglected if the boundary layer thickness is large compared to the radius of curvature. In the streamwise direction, this approximation is clearly justified and, in the spanwise direction, the ratio boundary layer thickness/radius is typically around 5%. Accounting for curvature in this direction leads to a decrease of the wall-pressure spectrum only in the subconvective domain [40]. At high subsonic Mach number, the modes that contribute to the panel response are predominantly excited by the convective elements of the boundary layer pressure field and so, neglecting the azimuthal curvature should not dramatically affect the response.

3.4.3. *Effects of the structural damping*

We will first examine how the structural dissipation affects the distribution of energy transferred from the flow to the panel. In order to show that this result is not specific to our parameter range, dimensionless forms of the power quantities involved in the balance energy equation (43) (Part I) are considered [38]. Figure 8 shows the spectral distribution of the dimensionless power quantities for a typical aircraft panel ($\zeta = 0{\cdot}01$).

We notice that only a small fraction of the power input incoming from the turbulent pressure field contributes to the radiated sound power. Most of the boundary layer input power is either dissipated within the structure or transmitted to the boundaries. As could be expected, this effect becomes more significant with increasing frequency, since the radiation damping effect decreases with frequency. Thus, for the panel of interest, the input power is almost entirely dissipated within the structure above 800 Hz (see Figure 8). Simulations have also been carried out for a lightly damped panel ($\zeta = 0{\cdot}001$). In this case, similar

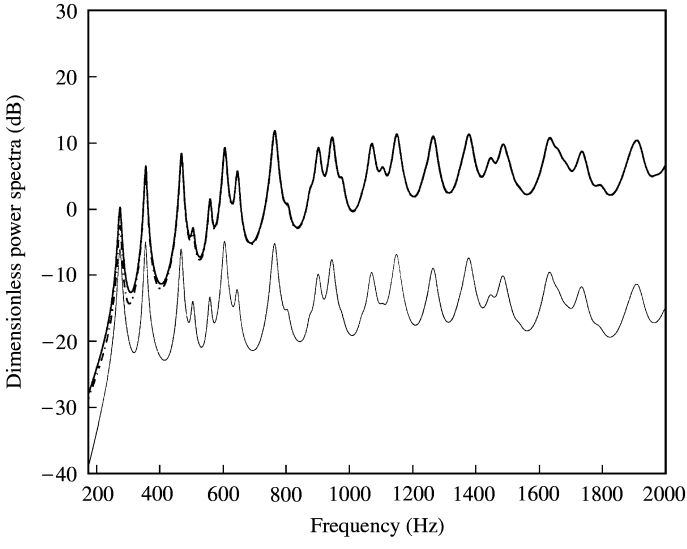

Figure 8. Energy balance of the power spectral quantities for an aircraft panel ($\zeta = 0{\cdot}01$): ———, boundary layer input power; - · - · -, structurally dissipated power; ——, inwardly radiated power.

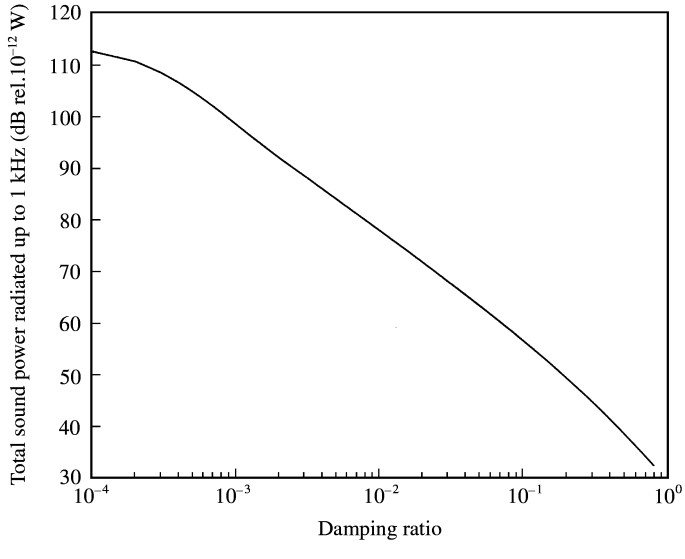

Figure 9. Influence of an increased structural damping on the total sound power inwardly radiated by the aircraft panel up to 1 kHz.

trends are observed but the structural damping becomes the dominant effect only above 1 kHz [38].

A second point is regarding how to use the structural damping effect to reduce flow-induced vibrations and radiation. Figure 9 shows that doubling the damping ratio of the panel provides a 6 dB attenuation for the levels of the total sound power radiated, here calculated up to 1 kHz. The same trend has been observed when the total sound power radiated is calculated up to 2 kHz. This effect of structural damping on the panel response can be understood since resonant modes contribute to the panel response over this

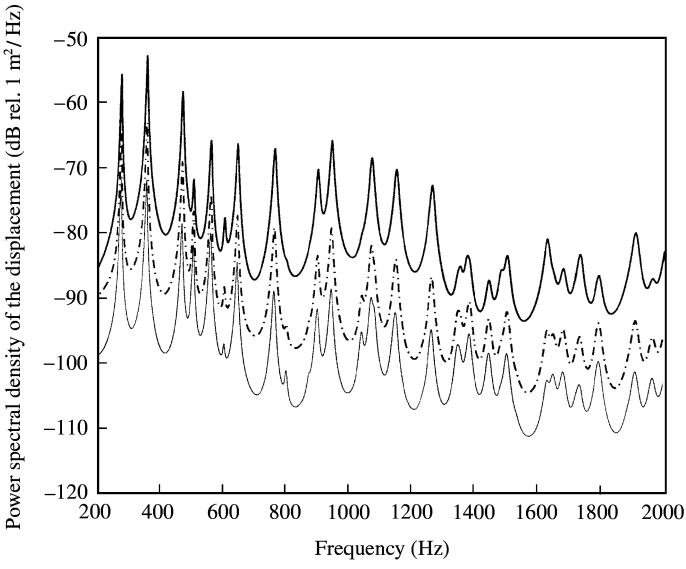

Figure 10. Influence of an increased flow velocity on the spectral density of the panel displacement normalized by the point-power spectrum of the TBL excitation: ———, $U_\infty = 225$ m/s; - · · · -, $U_\infty = 130$ m/s; ——, $U_\infty = 70$ m/s.

frequency range and the peak levels are $1/\zeta_{mn}^2$ dependent. Thus, increasing the damping ratio initially has a very beneficial influence on the total sound power radiated. However, as noticed by Graham [11], the same increment for higher values of the damping ratio brings diminishing returns.

3.4.4. *Hydrodynamic coincidence effect*

This important effect has been thoroughly discussed in references [6, 20] and we illustrate here its influence on the panel structural response. Figure 10 shows, for a fluid velocity varying from 70 to 225 m/s, the normalized spectral density of the panel displacement at the point (x_0, y_0). It is scaled onto the point-power spectrum of the wall-pressure fluctuations so that the increase of the noise source levels with the flow velocity does not appear. It can be seen that the bandwidth within which the vibration energy is contained increases with flow velocity. The explanation lies in the *hydrodynamic coincidence effect* that occurs over a frequency range for which each modal wavelength in the flow direction, $2a/n$, nearly coincides with the convecting scale of the turbulent excitation, $2\pi U_c/\omega$, where the main fluctuating energy lies.

Considering the case of an untensioned infinite plate excited by a turbulent flow provides a guideline to estimate the frequency ω_c below which hydrodynamic coincidence occurs. It is shown in Appendix A2 that the hydrodynamic wavenumber, $k_h = \omega/U_c$, matches the plate bending wavenumber, $\lambda_b = (m\omega^2/D)^{1/4}$, at the hydrodynamic coincidence frequency $\omega_c = U_c^2\sqrt{m/D}$. For the three flow velocities considered in Figure 10 (225, 130 and 70 m/s), the hydrodynamic coincidence frequencies are, respectively, 2540, 847 and 245 Hz and provide an upper limit above which no structural modes can be efficiently excited by the turbulent pressure field. However, we have to bear in mind that these frequencies overestimate the hydrodynamic frequency range in the case of a tensioned panel. Indeed,

because of pressurization effects, the panel resonance frequencies are shifted up and the hydrodynamic coincidence frequency range is consequently reduced.

Thus, the hydrodynamic coincidence effect enables us to explain as to why the vibration levels increase with flow velocity more rapidly than the noise source levels. For the aircraft panel of interest in contact with a high-speed subsonic flow, hydrodynamic coincidence exists up to 1·5 kHz. Note that, for an untensioned panel, it occurs over a broader frequency range (up to 2 kHz) since the number of modes efficiently excited by the convected field is more important.

3.4.5. *Modal radiation properties*

The third major effect which governs the amplitudes of the resonance peaks for the sound radiated is related to the radiation efficiency of each structural mode. From Table 2, it is clear that most of the modes which contribute to the response of the system are inefficient radiators at their resonant frequencies. This means that, below their critical frequency, these modes have large differences in their contribution to the farfield radiated pressure, the less efficient modes being the even–even modes. Above their critical frequency, however, these modes radiate sound independently, with an efficiency that asymptotes to one for all modes. For instance, we notice in Figure 7 that, below 500 Hz and for the untensioned panel, the resonant modes with the highest contribution to the sound power radiated are odd–odd inefficient modes. However, the (2,2) mode that does not contribute to the sound power radiated by the untensioned panel at its natural frequency of 232 Hz, because it is so inefficient, begins to radiate efficiently when the panel is tensioned and its frequency is raised to 494 Hz.

Another important point is that, below the critical frequency of each mode, the sound field radiated by this mode generally couples with any other structural mode. However, in the case of an excitation by a turbulent pressure field and above the transition frequency ω_T defined in section 3.2.2, the sound fields due to different structural modes are uncorrelated and so, the sound power radiated by the panel is just the sum of the sound power radiated by each structural mode. As discussed by the authors in reference [41], we are then certain to reduce the total sound power radiated by the plate if we manage to reduce the amplitude of any single structural mode, whereas this is not necessarily the case under a general harmonic excitation [42].

4. COMPARISONS WITH EXPERIMENTAL RESULTS

In this section, predictions, obtained from our model, are compared with experimental results performed in the anechoic wind-tunnel of the LMFA (Ecole Centrale de Lyon, France) for the vibration of a flat plate excited by a turbulent boundary layer [20].

A thin (1 mm thick) rectangular untensioned plate made of stainless steel was clamped on the rigid wall of a wind-tunnel test section. Although measurements were taken for flow velocities varying from 40 to 130 m/s, we only present the results obtained for the highest flow speed. Indeed, we have explained in section 2 as to why a Corcos-like model is not a good candidate for low subsonic flow applications and so, the experimental configuration with the highest flow speed seems more appropriate to assess the validity of our predictions when using a Corcos model for the excitation.

The plate was flush-mounted far downstream from the rectangular pipe inlet, in order to achieve conditions of homogeneity and stationarity for the airflow when developed over one side of the plate. The anechoic wind-tunnel has been designed to prevent the effects of

TABLE 3

Physical characteristics of the TBL-excited plate used in the experiments of Robert

Panel parameters	Flow parameters
Dimensions: $a \times b \times h = 0{\cdot}30 \times 0{\cdot}15 \times 0{\cdot}001\ \mathrm{m}^3$	Boundary layer thickness: $\delta = 0{\cdot}03$ m
Mass density: $\rho = 7800\ \mathrm{kg/m}^3$	Mass density: $\rho_+ = \rho_- = 1{\cdot}3\ \mathrm{kg/m}^3$
Young's modulus: $E = 200$ GPa	Sound speed: $c_+ = c_- = 340$ m/s
Modal damping ratio: $\zeta = 0{\cdot}005$	Free-stream velocity: $U_\infty = 130$ m/s
The Poissons' ratio: $\nu = 0{\cdot}3$	

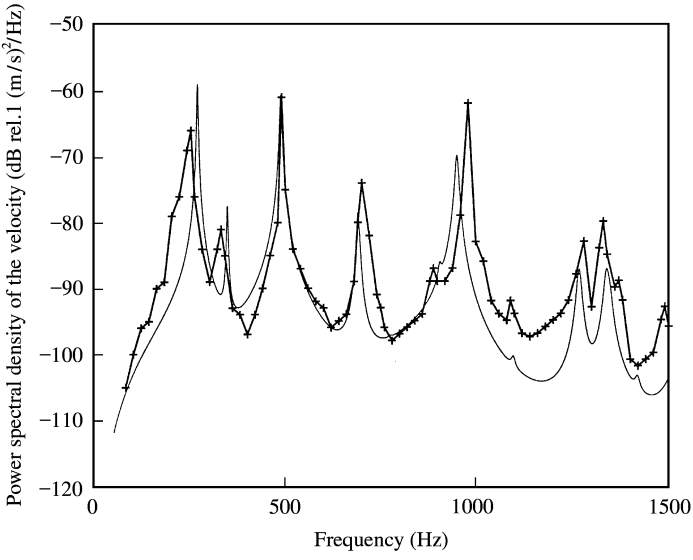

Figure 11. The power spectral density of the velocity, at the point $R1$, of a clamped plate excited by a turbulent boundary layer: comparisons between measurements performed by G. Robert (———) and predictions obtained using our modal formulation (——).

acoustic contamination from the centrifugal blower and the ambient noise. However, inaccuracies in the measurements below 200 Hz are attributed to an undesirable acoustic component due to the contribution of the longitudinal modes that are excited in the pipe between the inlet and the outlet. No noise cancellation techniques have been applied for the measurements presented here.

The plate acceleration was measured by small accelerometers attached to the structure. As the surface mass of the plate is high ($7{\cdot}8\ \mathrm{kg/m}^2$), the added mass effect introduced by the accelerometers can be neglected. The geometrical and mechanical characteristics of the system under study are summarized in Table 3.

In Figures 11 and 12, the experimental results (bold line) have been obtained by Robert [20] and the numerical ones (thin line) have been calculated by the authors with the modal formulation detailed in section 3 of Part I, but applied to the case of a clamped plate. The wavenumber sensitivity function for the clamped–clamped rectangular panel has been obtained by spatially Fourier transforming the Warburton analytical approximation of the panel structural modes [43, 44]. In Figure 11, we have plotted the measured and predicted power spectral density of the plate velocity at the point $x = 0{\cdot}08$ m and $y = 0{\cdot}16$ m, i.e., near

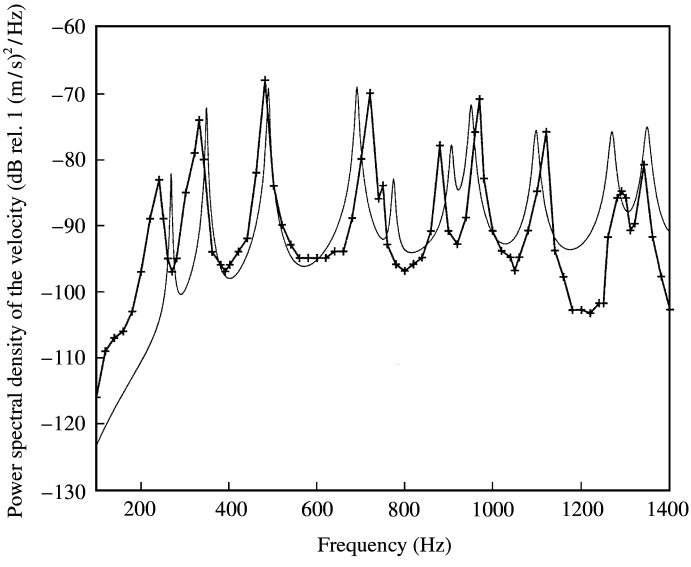

Figure 12. The power spectral density of the velocity, at the point R2, of a clamped plate excited by a turbulent boundary layer: comparisons between measurements performed by G. Robert (———) and predictions obtained using our modal formulation (——).

the centre of the plate. One can see that the overall levels at the peaks are correctly described by our model when using a damping ratio $\varsigma = 0{\cdot}005$, as suggested in reference [20]. Some small peaks have been detected and predicted above 800 Hz: they correspond to even–even modes that poorly contribute to the vibrating response of the plate measured at this position.

Measurements have also been performed at another point, with co-ordinates $x = 0{\cdot}09$ m and $y = 0{\cdot}27$ m, i.e., located near one corner of the plate. In this case, a larger number of modes are observed (see Figure 12). Thus, this configuration is more interesting in order to assess our model. We note that we have a better agreement with these experimental data than with the previous one, not only concerning the overall levels, but also when we compare the relative contribution of each peak to the vibrating response.

The differences concerning the position of the resonant peaks in Figures 11 and 12 are partly due to the errors inherent to the measurements of the mechanical parameters of the plate. However, the main source of errors could result from the fact that we have considered idealized boundary conditions (clamped plate) in our model and these boundary conditions are only approximated in the experiment.

5. CONCLUSIONS

In this paper, we have applied the general formulation presented in Part I for the response of a randomly excited panel to the prediction of the vibrations and the acoustic radiation of an aircraft fuselage panel using the tensioned flat plate model.

The requirements that have been derived in Part I for the neglect of the acoustic and the excitation modal coupling have been discussed *a posteriori*. They provide a good estimation for the validity range of the simplifying assumptions in case of an untensioned panel. When we account for pressurization effects, a more specific condition should be obtained to estimate the frequency below which fluid-loading effects can be neglected.

Parametric studies have pointed out the influence of the structural dissipation together with the hydrodynamic coincidence on the structural and acoustic response of the panel. First, increasing the structural damping reduces the levels of noise inwardly radiated. Second, the radiated sound power increases more rapidly with flow velocity than the turbulent pressure levels.

As outlined in section 3 while examining the modal radiation properties of an aircraft panel, we can consider that, under cruise condition, each structural mode radiates sound independently and so, a suitable strategy for the active structural acoustic control of the sound power inwardly radiated by the panels would be independent feedback control of each panel mode in the low-frequency domain.

Finally, good agreement is demonstrated between our predictions and previous experimental results which enables to show the validity of our simplified formulation. This model will be considered by the authors as a basis for a study of the boundary layer noise transmitted through aircraft sidewalls a typical configuration of which is a double panel partition containing a light insulating material.

ACKNOWLEDGMENTS

The authors would like to thank the anonymous reviewers for their helpful and insightful comments. The first author was supported by EPSRC grant no. N21529.

REFERENCES

1. J. S. Mixson and J. F. Wilby 1991 *NASA Reference Publication* 1258, *WRDC Technical Report* 90–3052. Aeroacoustics of flight vehicles: theory and practice. Volume 2: Noise Control, 271–355.
2. P. O. A. L. Davies 1996 *Journal of Sound and Vibration* **190**, 345–362. Aeroacoustics and time-varying systems.
3. J. C. Hardin 1976 *AGARD Lecture Series No.* 80 *on aerodynamic noise*. Airframe self-noise—four years of research.
4. I. Dyer 1959 *Journal of the Acoustical Society of America* **31**, 922–928. Boundary layer induced flow noise.
5. H. G. Davies 1971 *Journal of the Acoustical Society of America* **55**, 213–219. Sound from turbulent boundary layer excited panels.
6. W. R. Graham 1996 *Journal of Sound and Vibration* **192**, 101–120. Boundary layer induced noise in aircraft. Part I: the flat plate model.
7. W. V. Bhat 1971 *Journal of Sound and Vibration* **14**, 439–457. Flight test measurement of exterior turbulent boundary layer pressure fluctuations on Boeing model 737 airplane.
8. J. F. Wilby and F. L. Gloyna 1972 *Journal of Sound and Vibration* **23**, 443–466. Vibration measurements of an airplane fuselage structure. Part I: turbulent boundary excitation.
9. W. R. Graham 1995 *Journal of the Acoustical Society of America* **98**, 1581–1595. The influence of curvature on the sound radiated by vibrating panels.
10. L. Cremer, M. Heckl and E. E. Ungar 1988 *Structure-borne Sound*. Berlin: Springer-Verlag, second edition.
11. W. R. Graham 1996 *Journal of Sound and Vibration* **192**, 121–138. Boundary layer induced noise in aircraft. Part II: the trimmed flat plate model.
12. A. Cummings, H. J. Rice and R. Wilson 1999 *Journal of Sound and Vibration* **221**, 143–167. Radiation damping in plates, induced by porous media.
13. K. H. Lyle and E. H. Dowell 1994 *Journal of Fluids and Structures* **8**, 711–746. Acoustic radiation damping of flat rectangular plates subjected to subsonic flows. Parts I and II.
14. S. F. Wu and L. Maestrello 1995 *Journal of the American Institute of Aeronautics and Astronautics* **33**, 13–19. Responses of finite baffled plate to turbulent flow excitations.
15. R. L. Clark and K. D. Frampton 1997 *Journal of the Acoustical Society of America* **102**, 1639–1647. Aeroelastic structural acoustic coupling: implications on the control of turbulent boundary-layer noise transmission.

16. P. L. SHAH and M. S. HOWE 1996 *Journal of Sound and Vibration* **197**, 103–115. Sound generated by a vortex interacting with a rib-stiffened elastic plate.
17. M. S. HOWE 1989 *Journal of Fluids and Structures* **83**, 83–96. Sound produced by turbulent boundary layer flow over a finite region of wall roughness, and over a forward facing step.
18. M. S. HOWE 1998 *Journal of Sound and Vibration* **209**, 519–530. On the contribution from skin steps to boundary-layer generated interior noise.
19. F. HAN, R. J. BERNHARD and L. G. MONGEAU 1999 *Journal of Sound and Vibration* **227**, 685–709. Prediction of flow-induced structural vibration and sound radiation using energy flow analysis.
20. G. ROBERT 1984 *Thèse No*. 84-02, *Ecole Centrale de Lyon*, *France*. Modélisation et simulation du champ excitateur induit sur une structure par une couche limite turbulente.
21. S. BANO, R. MARMEY, L. JOURDAN and J.-P. GUIBERGIA 1992 *Journal d'Acoustique* **5**, 99–124. Etude théorique et expérimentale de la réponse vibro-acoustique d'une plaque couplée à une cavité en fluide lourd.
22. L. MAESTRELLO 1967 *Journal of Sound and Vibration* **5**, 407–448. Use of turbulent model to calculate the vibration and radiation responses of a panel, with practical suggestions for reducing sound levels.
23. H. G. DAVIES 1971 *Journal of Sound and Vibration* **15**, 107–126. Low frequency random excitation of water-loaded rectangular plates.
24. M. S. HOWE 1988 *Journal of Sound and Vibration* **121**, 47–65. Diffraction radiation produced by turbulent boundary layer excitation of a panel.
25. W. R. GRAHAM 1995 *Proceedings of the Royal Society of London A* **352**, 1–43. High-frequency vibration and acoustic radiation of fluid-loaded plates.
26. P. H. WHITE 1966 *Journal of the Acoustical Society of America* **40**, 1354–1362. Transduction of boundary-layer noise by a rectangular panel.
27. N. C. MARTIN and P. LEEHEY 1977 *Journal of Sound and Vibration* **52**, 95–120. Low wavenumber wall pressure measurements using a rectangular membrane as a spatial filter.
28. Y. F. HWANG and G. MAIDANIK 1990 *Journal of Sound and Vibration* **142**, 135–152. A wavenumber analysis of the coupling of a structural mode and flow turbulence.
29. A. O. BORISYUK and V. T. GRINCHENKO 1997 *Journal of Sound and Vibration* **204**, 213–237. Vibration and noise generation by elastic elements excited by a turbulent flow.
30. B. M. EFIMTSOV 1982 *Soviet Physics Acoustics* **28**, 289–292. Characteristics of the field of turbulent wall pressure fluctuations at large Reynolds numbers.
31. M. K. BULL 1996 *Journal of Sound and Vibration* **190**, 299–315. Wall-pressure fluctuations beneath turbulent boundary layers: some reflections on forty years of research.
32. W. R. GRAHAM 1997 *Journal of Sound and Vibration* **206**, 541–565. A comparison of models for the wavenumber–frequency spectrum of turbulent boundary layer pressures.
33. G. M. CORCOS 1963 *Journal of the Acoustical Society of America* **35**, 192–199. Resolution of pressure in turbulence.
34. C. DURANT, G. ROBERT, P. J. T. FILIPPI and P.-O. MATTEI 2000 *Journal of Sound and Vibration* **229**, 1115–1155. Vibroacoustic response of a thin cylindrical shell excited by a turbulent internal flow: comparison between numerical prediction and experimentation.
35. W. K. BLAKE 1986 *Mechanics of Flow-Induced Sound and Vibration*: *Complex Flow-Structure Interactions*, II. New York: Academic Press.
36. D. M. CHASE 1980 *Journal of Sound and Vibration* **70**, 29–67. Modelling the wavevector–frequency spectrum of turbulent boundary layer wall-pressure.
37. L. R. KOVAL 1976 *Journal of the Acoustical Society of America* **59**, 1379–1385. Effect of air flow, panel curvature and internal pressurization on field-incidence transmission loss.
38. C. MAURY, P. GARDONIO and S. J. ELLIOTT 2000 *ISVR Technical Report No*. 287. Model for the control of the sound radiated by an aircraft panel excited by a turbulent boundary layer.
39. R. D. BLEVINS 1984 *Formulas for Natural Frequency and Mode Shape*. (E. Robert editor). Malabar, FL: Krieger.
40. J. C. NEVES, P. MOIN and R. D. MOSER 1994 *Journal of Fluid Mechanics* **272**, 349–381. Effects of convex transverse curvature on wall-bounded turbulence. Part 1. The velocity and vorticity.
41. C. MAURY, P. GARDONIO and S. J. ELLIOTT 2001 *American Institute of Aeronautics and Astronautics Journal* **39**, 1860–1867. Active control of the flow-induced noise transmitted through a panel.
42. S. J. ELLIOTT and M. E. JOHNSON 1993 *Journal of the Acoustical Society of America* **94**, 2194–2204. Radiation modes and the active control of sound power.

43. G. B. WARBURTON 1951 *Proceedings of the Institute of Mechanical Engineering* **168**, 371–384. The vibration of rectangular plates.
44. N. C. MARTIN 1976 *Ph.D. Thesis, Department of Mechanical Engineering, Massachusetts Institute of Technology*. Wavenumber filtering by mechanical structures.
45. P. J. T. FILIPPI 1985 *Journal of Sound and Vibration* **100**, 69–81. Sound radiation by baffled plates and related boundary integral equations.
46. P. J. T. FILIPPI, P.-O. MATTEI, C. MAURY, A. H. P. VAN DER BURGH and C. J. M. DE JONG 2000 *Journal of Sound and Vibration* **229**, 1157–1169. Sound transmission through a thin baffled plate: validation of a light fluid approximation with numerical and experimental results.
47. N. WIENER 1930 *Acta Mathematica* **55**, 117–258. Generalized harmonic analysis.
48. G. K. BATCHELOR 1953 *The Theory of Homogeneous Turbulence*. (Reissued in the Cambridge Science Classics series 1982 by Cambridge University Press).

APPENDIX A: INFINITE PLATE EXCITED BY A TURBULENT FLOW

In this appendix, we consider the problem of the vibro-acoustic response of a uniform fluid-loaded flat plate, of infinite extent and excited by the wall-pressure fluctuations associated with a homogeneous turbulent flow over plate, which is more tractable than the problem with a finite plate. The main purpose of this example is to provide some insight into the main results obtained in the parametric analysis and to give *a priori* estimation of the accuracy of the approximations introduced in Part I, section 3, and associated to our initial problem.

The notation adopted is that introduced in Part I of this paper. First, consider γ_b the infinite fluid-loaded plate Green function that satisfies the equation

$$(\Delta_x^2 - k_b^4)\gamma_b(\mathbf{x}) + \varepsilon k_b^4 \iint_\infty \mathscr{G}_\omega(\mathbf{x}-\mathbf{x}')\gamma_b(\mathbf{x}')\,\mathrm{d}^2\mathbf{x}' = \delta/D, \qquad \mathbf{x}\in\mathbf{R}^2$$

with $k_b^4 = m\omega^2/D$ and $\varepsilon = 2\rho_0/m$; the plate separates two fluid domains characterized by a density ρ_0 and a sound velocity c_0. The uniqueness of the solution is determined by a Sommerfeld condition at infinity. The Neumann Green function $\mathscr{G}_\omega$ is defined in Part I, section 2, equation (39). The spatial Fourier transform Γ_b of γ_b is readily obtained

$$\Gamma_b(\mathbf{k};\omega) = \frac{\mathrm{j}\alpha}{D[\,\mathrm{j}\alpha(k^4 - k_b^4) + \varepsilon k_b^4\,]}, \quad k = |\mathbf{k}|, \quad \alpha^2 = k_0^2 - k^2. \tag{A1}$$

$k_0 = \omega/c_0$ is the acoustic wavenumber in both fluid domains and k_b is the plate bending wavenumber.

We assume that the turbulent excitation is described by the wavevector–frequency spectrum $S_{p_b p_b}(\mathbf{k};\omega)$, an expression of which, using the Corcos model, is given by equation (1) in section 2. Because the infinite fluid-loaded plate is a space- and time-invariant system, its wavevector–frequency response, S_{ww}^{∞}, to a turbulent field is related to the excitation spectrum $S_{p_b p_b}$ by

$$S_{ww}^{\infty}(\mathbf{k};\omega) = |\Gamma_b(\mathbf{k};\omega)|^2\, S_{p_b p_b}(\mathbf{k};\omega). \tag{A2}$$

According to equations (A1) and (1),

$$S_{ww}^{\infty}(\mathbf{k};\omega) = \frac{\alpha^2}{D^2[\,\alpha^2(k^4 - k_b^4)^2 + \varepsilon^2 k_b^8\,]} \frac{L_y}{[(k_y - k_h)^2 L_y^2 + 1]} \frac{L_x}{[k_x^2 L_x^2 + 1]}\, \mathbf{\Phi}_0(\omega), \tag{A3}$$

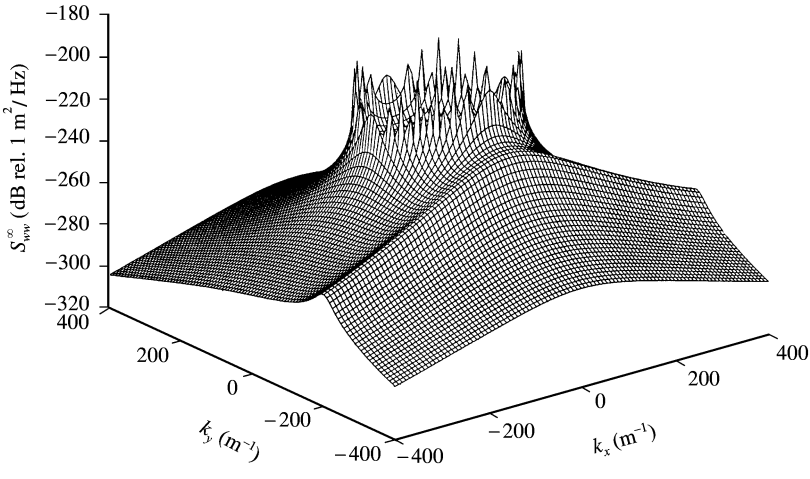

Figure A1. The power spectral density, $S^{\infty}_{ww}(\omega)$, of the displacement of an infinite aluminium plate excited by a turbulent airflow ($U_{\infty} = 225$ m/s) as a function of k_x and k_y and for an analysis frequency $f = 5$ kHz.

where $k_h = \omega/U_c$ stands for the hydrodynamic wavenumber and L_x, L_y for the spanwise and streamwise correlation lengths. In equation (A3), we notice that the wavevector–frequency spectrum of the displacement of the flow-excited plate is infinite-valued along the circle $|\mathbf{k}| = k_1$, where k_1 is one of the real roots of the dispersion equation of the fluid-loaded plate

$$\mathrm{j}\alpha(k^4 - k_b^4) + \varepsilon k_b^4 = 0. \tag{A4}$$

It corresponds to the free wavenumber of the fluid-loaded plate that propagates without losing energy into the fluid.

Moreover, a maximum occurs at $\mathbf{k} = (0, k_h)$ and corresponds to the spectral contribution of the convective peak. These features are illustrated in Figure A1 where the wavevector spectrum of the structural response of an infinite aluminium plate in contact with an airflow ($U_{\infty} = 225\,m$/s) is plotted as a function of k_x and k_y at a fixed frequency ($f = 5$ kHz) such that $k_1 \approx 1{\cdot}5\,k_0$, $k_h \approx 2{\cdot}2k_0$ and $k_0 \approx 100$. We see that the dominant contribution to the structural response of an infinite fluid-loaded plate excited by a turbulent airflow comes from wavevectors having magnitudes equal to k_1 and this holds whatever the analysis frequency and the flow velocity.

A noteworthy point is that the roots of the quintic equation (A4) are not known explicitly. However, inasmuch as the fluid has a small influence on the plate vibrations, as in our case, accurate analytical approximations of these roots can be obtained.

A.1. ACCURACY OF THE LIGHT FLUID APPROXIMATION

When the parameter ε is small, the roots of equation (A4) are close to $\pm k_b$, $\pm \mathrm{j}k_b$ and $\pm k_0$. Because the frequency range of interest is, in the case considered here, below the coincidence frequency $\omega_c = c_0^2\sqrt{m/D}$, defined by $k_0(\omega_c) = k_b(\omega_c)$ and which is equal to 8 kHz for the plate described in section 3, we will first assume that $k_0 < k_b$. The perturbation method can be applied to each regular root by posing a power series in ε starting with ε^0 as given by: $k \approx k_b(1 + \varepsilon\delta_1 + \varepsilon^2\delta_2 + \ldots)$. Thus substituting this

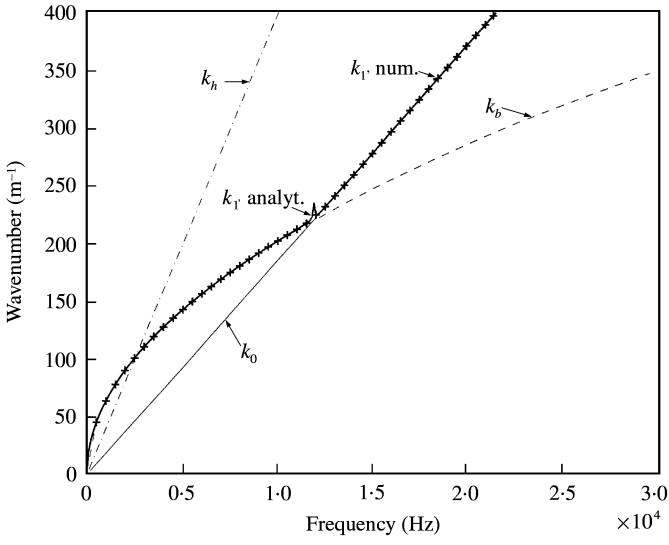

Figure A2. Wavenumbers frequency dependence for an infinite plate: ——, acoustic wavenumber k_0; - - - -, plate bending wavenumber k_b; - · - · -, hydrodynamic wavenumber, k_h; ——, first order analytical approximation of the real dispersion root k_1; xxxx, numerical approximation of the real dispersion root k_1.

expansion into equation (A4) yields

$$k_1 \approx k_b\left(1 + \frac{\varepsilon}{2\sqrt{k_b^2 - k_0^2}}\right).$$

Applying the same method to the other roots yields

$$k_{2,3} \approx \mathrm{j}k_b\left(1 \pm \frac{\mathrm{j}\varepsilon}{2\sqrt{k_b^2 + k_0}}\right), \quad k_{4,5} \approx k_0\left(1 \pm \frac{\mathrm{j}\varepsilon k_b^4}{k_0^2(k_b^4 - k_0^4)}\right).$$

In the case $k_0 > k_b$, the perturbation method leads to

$$k_1 \approx k_0\left(1 + 2\varepsilon^2\left(\frac{k_b^4}{k_0(k_0^4 - k_b^4)}\right)^2\right), \quad k_{2,3} \approx \mathrm{j}k_b\left(1 \pm \frac{\mathrm{j}\varepsilon}{2\sqrt{k_b^2 + k_0^2}}\right),$$

$$k_{4,5} \approx k_b\left(1 \pm \frac{\mathrm{j}\varepsilon}{2\sqrt{k_0^2 - k_b^2}}\right).$$

We now have asymptotic approximations for each root of the dispersion relation. Their accuracy is determined by the last term included once ε is sufficiently small. As depicted in Figure A2, accounting for the two first leading order terms already provides, in our range of parameters, a very accurate approximation of the real root k_1, but away from the coincidence frequency. An asymptotic representation uniformly valid over the whole frequency range would require first an inner approximation for the roots, only valid at the vicinity of this particular frequency and then, to assume that the inner and outer expansions are of a similar form in an overlap area (matched asymptotic expansion). Restricting our attention to frequencies below ω_c, it appears that the accuracy of the zero order approximation for the real dispersion root is governed by the smallness of the quantity $\varepsilon k_b/2\sqrt{k_b^2 - k_0^2}$.

Furthermore, the inverse Fourier transform of equation (A1) yields an exact expression of the plate displacement γ_b in terms of the roots of the dispersion relation [45]. Substituting the roots approximations into this expression and comparing with the first order approximation of the solution enables one to show that the four following parameters govern the accuracy of the first order expansion for the structural response of an infinite fluid-loaded plate [46]:

$$\frac{\varepsilon k_b}{4\sqrt{k_b^2 - k_0^2}}, \quad \frac{\varepsilon k_b |\mathbf{x}|}{4\sqrt{k_b^2 - k_0^2}}, \quad \frac{\varepsilon k_b}{4\sqrt{k_b^2 + k_0^2}}, \quad \frac{\varepsilon k_b |\mathbf{x}|}{4\sqrt{k_b^2 + k_0^2}}. \tag{A5}$$

First, we notice that these criteria are general and do not depend on the nature of the excitation. Second, as suggested in reference [46], one can reasonably assume that their validity condition is independent of the plate boundary conditions and/or geometry and so, are of the same order of magnitude as for a finite-dimensional plate.

A.2. SIMPLIFICATION OF THE SPECTRAL DENSITY FOR THE FLOW-INDUCED DISPLACEMENT OF THE PLATE

The validity condition of this simplification is easily obtained in the space–frequency domain. Thus let us consider the inverse spatial Fourier transform of equation (A2). We then obtain an expression similar to expression (24) (see Part I, section 2) for the spectrum of the plate displacement:

$$S_{ww}^{\infty}(\Xi;\omega) = \iint_{\infty} \iint_{\infty} \gamma_b(\mathbf{x};\omega)\, S_{p_b p_b}(\Xi - \mathbf{x} + \mathbf{x}';\omega)\, \gamma_b^*(\mathbf{x}';\omega)\, \mathrm{d}^2\mathbf{x}\, \mathrm{d}^2\mathbf{x}'. \tag{A6}$$

We note that, inasmuch as the spectrum of the excitation does not depend on the location $\mathbf{x}$, the spectrum of the displacement of the infinite plate depends only on the separation Ξ. Introducing the new variable $\mathbf{v} = \Xi - \mathbf{x} + \mathbf{x}'$ into (A6) yields

$$S_{ww}^{\infty}(\Xi;\omega) = \iint_{\infty} \iint_{\infty} \gamma_b(\mathbf{x};\omega)\, \gamma_b^*(\mathbf{x} - \Xi\mathbf{v};\omega)\, S_{p_b p_b}(\mathbf{v};\omega)\, \mathrm{d}^2\mathbf{x}\, \mathrm{d}^2\mathbf{v}.$$

This expression can be factorized in the form:

$$S_{ww}^{\infty}(\Xi;\omega) \approx \Phi_0(\omega) \left[\iint_{\infty} \gamma_b(\mathbf{x};\omega)\, \gamma_b^*(\mathbf{x}\Xi;\omega)\, \mathrm{d}^2\mathbf{x} \right], \tag{A7}$$

where $\boldsymbol{\Phi}_0$ is the *point power spectrum* or *correlation area* of the excitation, which is defined in the wavenumber domain by equation (2) and, in the space–frequency domain, by $\boldsymbol{\Phi}_0(\omega) = \iint_{\infty} S_{p_b p_b}(\Xi;\omega)\, \mathrm{d}^2\Xi$. The simplification of equation (A6) into equation (A7) is only valid when $\boldsymbol{\Phi}_0(\omega) \ll 4\pi^2/\lambda_b^2(\omega)$, i.e., when the greatest area along which the turbulent field is correlated is small compared to the square of the structural wavelength and so, when the structure does not accept a lot of energy from the flow.

For a finite dimensional plate, a similar simplification occurs when the correlation area is smaller that the plate surface [5], but a more stringent condition could be formulated in terms of each modal wavelength. In any case, such simplification enables a lot of computational effort to be saved.

Finally, we notice that, if we introduce a structural damping, the amount of flow energy accepted by the structure strongly depends on this parameter and this point is discussed for the case of a finite dimensional plate in section 3.

A.3. DIRECT FOURIER ANALYSIS OF THE PLATE RESPONSE

As outlined at the beginning of Part I, section 2, many authors write the equations governing the response of any continuous linear system to a general random forcing in the space–frequency domain or in the wavenumber–frequency domain, assuming that each realization of the response satisfies the condition for a Fourier integral to exist. However, it is not likely that a strongly, or even a weakly stationary and homogeneous process is, in some way, "localized" in time and space and so, possesses a classical Fourier transform.

An important result due to Wiener [47] is that, whereas the Fourier transform of a random event $w(\mathbf{x}, t)$ occurring on a volume V and over a period of time $[0, T]$ diverges as V and T tend to infinity, the limit of its integral on the infinitesimal dual domain, which we note as $\mathrm{d}W(\mathbf{k}; \omega)$, exists when $V, T \to \infty$. Each particular realization of the process can then be written in terms of the random increment $\mathrm{d}W(\mathbf{k}; \omega)$ in the form

$$w(\mathbf{x}; t) = \iint_{\infty} \mathrm{e}^{\mathrm{j}(\omega t - \mathbf{k}; \omega)} \, \mathrm{d}W(\mathbf{k}; \omega). \tag{A8}$$

Expression (A8) is a Fourier–Stieltjes integral accounting for unbounded variations of $W(\mathbf{k}; \omega)$. Considering the spectral density of the random increment, it is found, as shown in reference [48], that

$$\lim_{\mathrm{d}\mathbf{k}, \mathrm{d}\omega \to 0} \frac{S_{\mathrm{d}W \, \mathrm{d}W}(\mathbf{k}; \omega)}{\mathrm{d}\mathbf{k} \, \mathrm{d}\omega} = \frac{1}{(2\pi)^3} \iint_{\infty} R_{ww}(\mathbf{x}; t) \, \mathrm{e}^{-\mathrm{j}(\omega t - \mathbf{k}; \mathbf{x})} \, \mathrm{d}x \, \mathrm{d}t.$$

$$= S_{ww}(\mathbf{k}; \omega). \tag{A9}$$

The same analysis can be applied to the turbulent excitation field $p_b(\mathbf{x}; t)$ and the difference $p_s(\mathbf{x}; t)$ between the surface pressure fields radiated in each fluid domain. For instance, for the forcing field, it reads as

$$p_b(\mathbf{x}; t) = \iint_{\infty} \mathrm{e}^{\mathrm{j}(\omega t - \mathbf{k}; x)} \, \mathrm{d}\mathbf{P}_b(\mathbf{k}; \omega), \tag{A10}$$

$$\lim_{\mathrm{d}\mathbf{k}, \mathrm{d}\omega \to 0} \frac{S_{\mathrm{d}P_b, \mathrm{d}P_b}(\mathbf{k}; \omega)}{\mathrm{d}\mathbf{k} \, \mathrm{d}\omega} = S_{p_b p_b}(\mathbf{k}; \omega). \tag{A11}$$

If we substitute equations (A8, A10) into the governing equation

$$\left(D\Delta_x^2 + m \frac{\partial^2}{\partial t^2} \right) w(\mathbf{x}; t) = p_b(\mathbf{x}; t) - p_s(\mathbf{x}; t)$$

one obtains

$$\left(k^4 - k_b^4 + \frac{\varepsilon k_b^4}{\mathrm{j}\alpha} \right) \mathrm{d}W(\mathbf{k}; \omega) = \frac{\mathrm{d}\mathbf{P}_b(\mathbf{k}; \omega)}{D}.$$

Evaluating the spectral density of the increments, according to equations (A9, A11), yields

$$S^{\infty}_{ww}(\mathbf{k};\omega) = \frac{\alpha^2}{D^2\left[\alpha^2(k^4 - k_b^4)^2 + \varepsilon^2 k_b^8\right]} S_{p_b p_b}(\mathbf{k};\omega).$$

i.e., the input–output relationship (A2) we have derived at the beginning of this appendix between the statistics of the wall-pressure field and the structural response of the plate, but using the superposition principle applied to a space- and time-invariant linear system.